Structural Insight into the Mechanism of Substrate Specificity of *Aedes* Kynurenine Aminotransferase[†,‡]

Qian Han,[§] Yi Gui Gao,[∥] Howard Robinson,[⊥] and Jianyong Li*[,§]

Department of Biochemistry, Virginia Tech, Blacksburg, Virginia 24061, School of Chemical Sciences, University of Illinois, Urbana, Illinois 61801, and Biology Department, Brookhaven National Laboratory, Upton, New York 11973

Received September 3, 2007; Revised Manuscript Received December 4, 2007

ABSTRACT: *Aedes aegypti* kynurenine aminotransferase (AeKAT) is a multifunctional aminotransferase. It catalyzes the transamination of a number of amino acids and uses many biologically relevant α-keto acids as amino group acceptors. AeKAT also is a cysteine S-conjugate *β*-lyase. The most important function of AeKAT is the biosynthesis of kynurenic acid, a natural antagonist of NMDA and α7-nicotinic acetylcholine receptors. Here, we report the crystal structures of AeKAT in complex with its best amino acid substrates, glutamine and cysteine. Glutamine is found in both subunits of the biological dimer, and cysteine is found in one of the two subunits. Both substrates form external aldemines with pyridoxal 5-phosphate in the structures. This is the first instance in which one pyridoxal 5-phosphate enzyme has been crystallized with cysteine or glutamine forming external aldimine complexes, cysteinyl aldimine and glutaminyl aldimine. All the units with substrate are in the closed conformation form, and the unit without substrate is in the open form, which suggests that the binding of substrate induces the conformation change of AeKAT. By comparing the active site residues of the AeKAT−cysteine structure with those of the human KAT I−phenylalanine structure, we determined that Tyr286 in AeKAT is changed to Phe278 in human KAT I, which may explain why AeKAT transaminates hydrophilic amino acids more efficiently than human KAT I does.

The sequence of *Aedes aegypti* kynurenine aminotransferase (AeKAT)[1] is 47% identical with that of human KAT I and 51.9% identical with that of human KAT III (*1*). Human, rat, and mouse KAT I enzymes have been extensively studied (*2*, *3*). Mammalian KAT I, also called glutamine transaminase K (GTK), is a multifunctional aminotransferase that acts on a number of amino acids (glutamine, cysteine, phenylalanine, kynurenine, methionine, etc.) and uses many biologically relevant keto acids as amino group acceptors (*3*, *4*). AeKAT and a glutamine:phenylpyruvate aminotransferase from *Thermus thermophilus*, homologues of mammalian KAT I, have also been systematically characterized (*5*, *6*). One of the enzymatic products of KAT I is kynurenic acid (KYNA), which is the only known endogenous antagonist of the *N*-methyl-D-aspartate (NMDA) subtype of glutamate receptors (*7*−*9*). KYNA is also the antagonist of the α7-nicotinic acetylcholine receptor (*10*−*12*). Very recently, KYNA has been identified as an endogenous ligand of an orphan G protein-coupled receptor (GPR35) that is predominantly expressed in immune cells (*13*). The tryptophan metabolic pathway is activated during inflammatory conditions, such as viral invasion, bacterial lipopolysaccharide, or interferon stimulation (*14*, *15*). The activation of tryptophan metabolism causes a reduced plasma tryptophan level and an elevated KYNA concentration (*16*). Therefore, this receptor−ligand pair may also play a role in immunological regulation.

Many other functions have been proposed for mammalian KAT I enzymes, including maintaining low levels of phenylpyruvate, closing the methionine salvage pathway, regulating α-keto acid levels, sparing the essential amino acids, and maintaining a continual equilibrium among the amino acids (*3*, *17*). However, quantitatively, the most important amine donor for KAT I enzymes in vivo is glutamine. The product of glutamine transamination (α-ketoglutaramate) is rapidly removed by cyclization and/or conversion to α-ketoglutarate. Transamination is therefore "pulled" in the direction of glutamine utilization (*3*). AeKAT showed high activity toward a number of amino acids, including glutamine, cysteine, tyrosine, methionine, phenylalanine, histidine, and kynurenine. Interestingly, cysteine has an intriguing effect on AeKAT activity toward kynurenine, enhancing its activity at relatively low concentrations and inhibiting its activity at higher concentrations (*5*, *18*). Crystal structures of AeKAT, glutamine:phenylpyruvate aminotransferase from *T. thermophilus*, and human KAT I have been available for substrate recognition study (*19*−*21*). They are fold type I aminotransferases (*22*, *23*), characterized by the

[†] This work was supported by Grant AI 44399 from the National Institutes of Health.

[‡] The atomic coordinates and structure factors (entries 2r5c and 2r5e) have been deposited in the Protein Data Bank.

* To whom correspondence should be addressed. Telephone: (540) 231-1182. Fax: (540) 231-9070. E-mail: lij@vt.edu.

[§] Virginia Tech.

[∥] University of Illinois.

[⊥] Brookhaven National Laboratory.

[1] Abbreviations: AeKAT, *Aedes aegypti* kynurenine aminotransferase; C6P, cysteinyl aldimine; KAT, kynurenine aminotransferase; KYNA, kynurenic acid; LLP, lysine pyridoxal 5′-phosphate; PLP, pyridoxal 5′-phosphate; QLP, glutaminyl aldimine; rmsd, root-mean-square deviation.

10.1021/bi701800j CCC: $40.75
Published on Web 01/11/2008

presence of an N-terminal arm, a small domain, and a large domain. However, complex structures with their best natural amino acid substrates (such as glutamine and cysteine) were unavailable. The crystal structure of AeKAT indicated that Cys284 in AeKAT might be the cysteine regulation target of AeKAT. Cys284 is located in the large domain of the subunit and forms a thiol−thiolate hydrogen bond with Cys284 from the other subunit. The cysteine pair is close to the active center of AeKAT. Under oxidative conditions, these cysteine residues in AeKAT can reasonably form a disulfide bond because of the short distance between the sulfur atoms, requiring only a decrease of 1.5−1.6 Å (*20*). To understand the structural basis underlying substrate recognition and catalysis, we determined the three-dimensional crystal structures of AeKAT in complex with its best specific substrates, cysteine and glutamine. This is the first time that the crystal structures of the enzyme−glutamine and enzyme−cysteine complexes of KAT I enzymes have been reported.

MATERIALS AND METHODS

Expression and Purification of Recombinant AeKAT. AeKAT lacking the NH_2-terminal mitochondrial leader sequence (amino acids 1−48) was expressed in a baculovirus/insect cell protein expression system and purified for crystallization (*18*, *20*). The purified recombinant AeKAT was concentrated to 10 mg/mL protein in 5 mM phosphate buffer (pH 7.5) using a Centricon YM-30 concentrator (Millipore).

AeKAT Crystallization. The crystals were grown via hanging drop vapor diffusion methods with the volume of reservoir solution at 500 μL and the drop volume at 2 μL, containing 1 μL of protein sample and 1 μL of reservoir solution based on the previous reported method (*20*), except that the precipitant was changed from PEG 8000 to ammonium sulfate. The new crystallization buffer contained 2 M ammonium sulfate and 0.1 M Tris at pH 8.5. The AeKAT−cysteine complex was cocrystallized by adding 2.5 mM L-cysteine to the crystallization buffer described above. The crystals of the glutamine−enzyme complex were obtained by soaking the AeKAT crystals overnight in 2.5 mM L-glutamine in the crystallization buffer described above.

Data Collection and Processing. Individual AeKAT complex crystals were cryogenized in crystallization buffer containing 30% PEG 400 as a cryoprotectant. Diffraction data of AeKAT complex crystals were collected at Brookhaven National Synchrotron Light Source beamline X29A ($\lambda = 1.1$ Å). Data collection was carried out using an ADSC Q315 CCD detector. All data were indexed and integrated using HKL (*24*). Scaling and merging of diffraction data were performed using SCALEPACK (*25*). The parameters of the crystals and information regarding data collection are listed in Table 1.

Structure Determination. The structures of AeKAT complexes were determined by the molecular replacement method using the published AeKAT structure without any ligands or waters (Protein Data Bank entry 1YIY) (*20*). Molrep (*26*) in the CCP4 suite was employed to calculate both the cross-rotation and translation function of the model. The initial model was subjected to iterative cycles of crystallographic refinement with Refmac, version 5.2 (*27*), and graphic sessions for model building used O (*28*). The substrate molecules were modeled when the *R* factor dropped to a value of 0.23 at full resolution for the AeKAT−glutamine structure and a value of 0.24 at full resolution for the AeKAT−cysteine structure based on both the $2F_o - F_c$ and $F_o - F_c$ electron density maps. Solvent molecules were automatically added and refined with ARP/wARP (*29*) together with Refmac, version 5.2.

Table 1: Data Collection and Refinement Statistics

	AeKAT−glutamine	AeKAT−cysteine
Crystal Data		
space group	$P2_12_12_1$	
unit cell		
a (Å)	56.373	56.050
b (Å)	95.590	95.678
c (Å)	165.901	166.752
$\alpha = \beta = \gamma$ (deg)	90.000	90.000
Data Collection		
X-ray source	BNL[a] X29	
wavelength	1.1	1.1
resolution (Å)[b]	1.84 (1.91−1.84)	1.96 (2.03−1.96)
total no. of reflections	475345	455740
no. of unique reflections	78429	65484
R_{merge}[b]	0.077 (0.275)	0.072 (0.274)
redundancy[b]	6.7 (4.0)	7.4 (4.7)
completeness (%)[b]	90.2 (45.3)	94.4 (67.0)
Refinement Statistics		
R_{work} (%)[b]	20.1 (24.4)	21.8 (36.5)
R_{free} (%)[b]	24.3 (30.4)	26.7 (40.2)
rmsd for bond lengths (Å)	0.016	0.027
rmsd for bond angles (deg)	1.713	1.926
no. of ligand or cofactor molecules	2 QLP	1 LLP, 1 C6P
no. of water molecules	584	469
average overall *B* (Å^2)	32.8	42.5
Ramachandran plot		
allowed (%)	99.7	99.7
generously allowed (%)	0	0.0
disallowed (%)	0.3	0.3

[a] Brookhaven National Laboratory. [b] The values in parentheses are for the highest-resolution shell.

Structure Analysis. Superposition of structures was conducted using Lsqkab (*30*) from the CCP4 suite. Figures were generated using Pymol (*31*). Protein−substrate interaction was also analyzed using Pymol (*31*).

RESULTS

Overall Structure. The structures of AeKAT−substrate complexes were determined through molecular replacement and refined to 1.96 Å resolution for the AeKAT−cysteine complex and 1.84 Å resolution for the AeKAT−glutamine complex. The final models contain 419 residues in each subunit and yield a crystallographic *R* value of 21.1% and an R_{free} value of 24.3% for the AeKAT−glutamine complex and an *R* value of 21.8% and an R_{free} value of 26.7% for the AeKAT−cysteine complex with ideal geometry evaluated with Molprobity (http://molprobity.biochem.duke.edu/) (Table 1). There are two protein molecules in an asymmetric unit that form one biological homodimer. The residues of the two subunits in AeKAT complexes are numbered 11 (A)−429 (A) for chain A and 11 (B)−429 (B) for chain B. The results of the refinement are summarized in Table 1. All residues except Tyr286 in all four chains are in favorable regions of the Ramachandran plot as defined with Procheck (*32*).

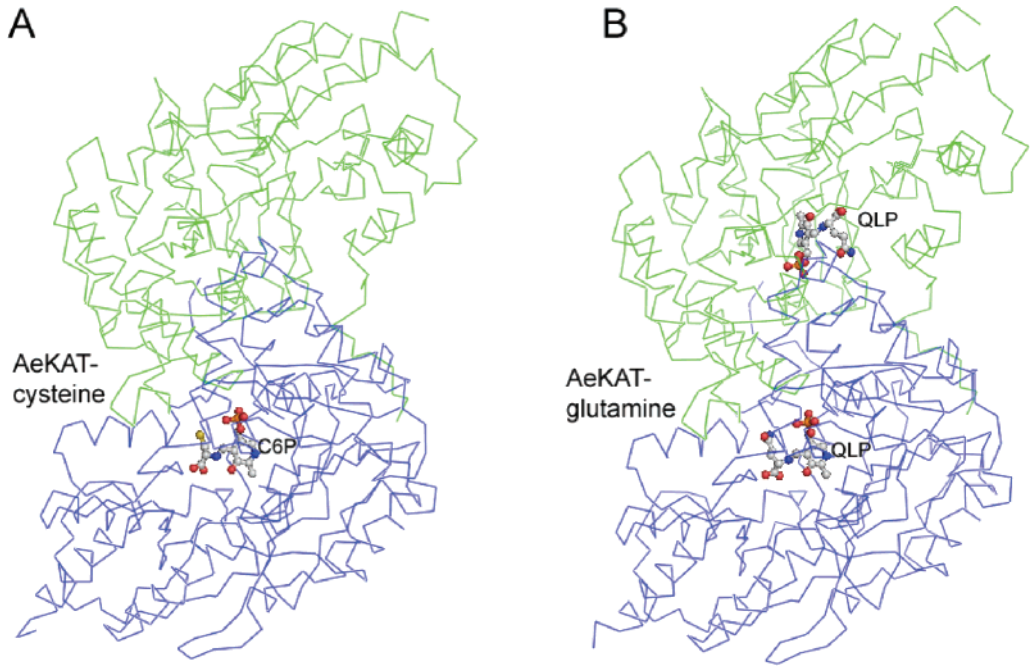

FIGURE 1: α-Carbon representation of the structures of AeKAT complexes: (A) AeKAT−cysteine complex and (B) AeKAT−glutamine complex.

Although Tyr286 (A) and (B) in all complex structures fall within a disallowed region of the Ramachandran plot of the determined structures, its excellent electron density allowed us to unambiguously assign the observed conformations (Figure 7A,B). Interestingly, Tyr286 (A) and (B) are in the favored region of the Ramachandran plot evaluated with Molprobity. The first 10 residues (1−10) were not defined in both the $2F_o - F_c$ and $F_o - F_c$ electron density maps and are absent from the final models. The protein architecture revealed by AeKAT complex structures remains the same as that of the native AeKAT structure previously described (*20*). Electron density consistent with the presence of glutamine was observed in the active sites of both subunits of the AeKAT−glutamine complex, whereas only one of the monomers in the AeKAT−cysteine complex exhibited electron density consistent with the presence of cysteine (Figure 1). By binding the substrates, the protein chains changed their conformations to the closed forms in the AeKAT−glutamine complex. Similarly, chain B in the AeKAT−cysteine complex also assumed a closed form, but chain A without the ligand remained as the open form (chain A in the AeKAT−cysteine complex).

Substrate Recognition and Catalysis in the AeKAT−Cysteine Complex. Inspection of the crystal structure of the AeKAT−cysteine complex revealed that the substrate lies near the PLP cofactor and forms an external aldimine with PLP. However, cysteine is seen in only one of the two subunits in a biological dimer. There are three water molecules at the active site of the subunit that do not contain a cysteine molecule and two waters in the subunit that contains a cysteine. A water molecule (W206) forms a hydrogen bond (3.6 Å) with the SG atom of C6P and also interacts with the NZ atom of Lys263 (2.7 Å), the OH atom of Tyr73 (A chain) (3.6 Å), and the OP2 atom of C6P (3.1 Å). Another water molecule (W368) forms a hydrogen bond (3.4 Å) with the O atom of C6P and also interacts with Gly45 (3.3 Å), Tyr340 (2.9 Å), and Tyr224 (2.9 Å). Several

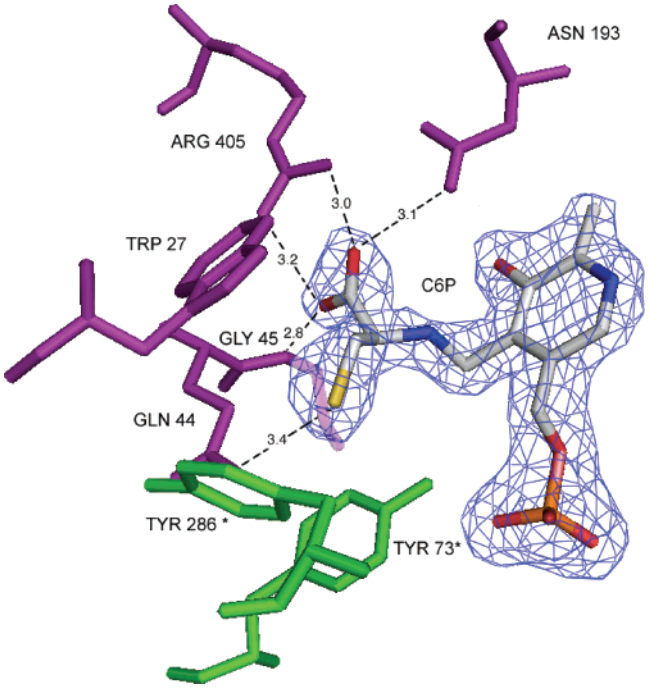

FIGURE 2: Cysteine binding site. The cysteinyl aldimine (C6P) and the protein residues within 4 Å of cysteine substrate are shown. Residues colored pink are from chain B and residues colored green from chain A. The $2F_o - F_c$ electron density map covering C6P is shown contoured at the 1.3σ level. This figure was generated with PyMol.

residues, including Arg405 (B), Tyr224 (B), Asn193 (B), Gln44 (B), Gly45 (B), Trp27 (B), Tyr73 (A), and Phe135 (B), define the substrate-binding site and contact the cysteine molecule. The carboxylate of cysteine forms a salt bridge with the guanidinium group of Arg405. The salt bridge is fixed by hydrogen bonding interactions with the NH atom of Gly45 (B) and the side chain of Asn193 (B) at both sides of the salt bridge. Gln44 (B) and Gly45 (B) are located at the turning point of the loop that dives into and partially

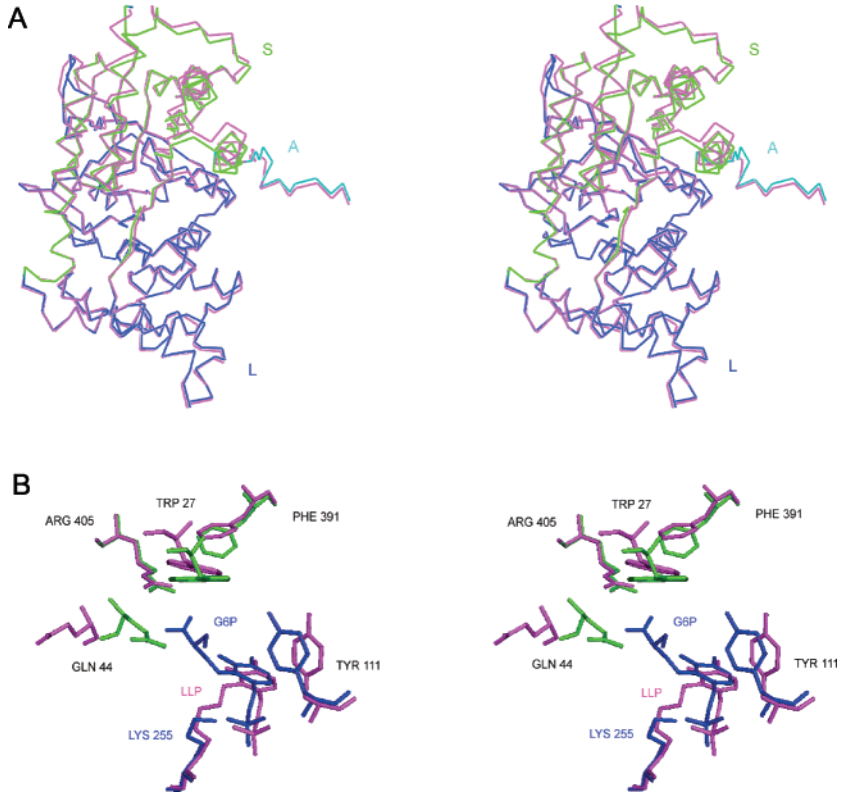

FIGURE 3: (A) α-Carbon representation in stereo of chain B (closed form) superimposed onto chain A (open form, colored pink) of the AeKAT−cysteine complex. The small domain (S), arm (A), and large domain (L) are colored blue, green, and light blue, respectively. (B) Superposition of chain B onto chain A of the AeKAT−cysteine complex. Only protein residues having different conformations within 5 Å of the cysteine substrate are depicted as sticks. The residues and ligand from chain A are colored pink and those from chain B colored green or blue.

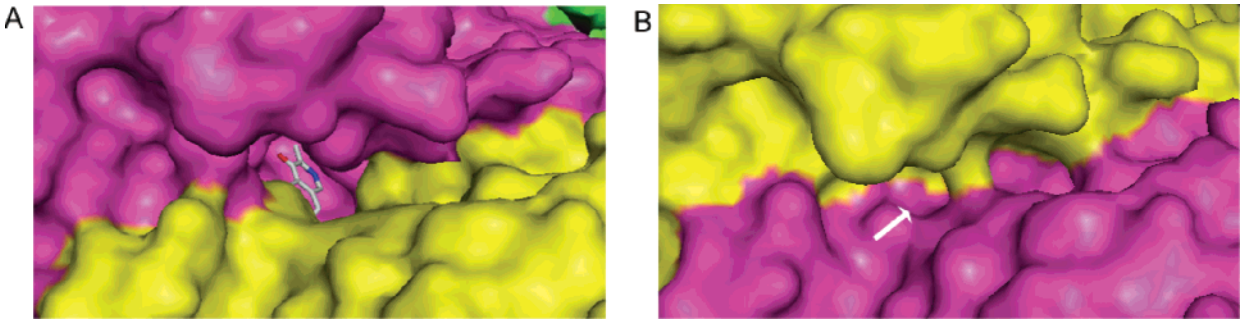

FIGURE 4: Molecular surface of the AeKAT−cysteine complex. (A) Surface around the active center of the open form, chain A. The built-in cavity is clearly seen, and the cofactor is seen through the tunnel. (B) Surface around the active center of the closed form, chain B. The built-in cavity is much smaller than the cavity in the open form, and the tunnel to the cofactor is closed.

plugs the enzyme active site, thus shielding the substrate-binding pocket from the bulk solvents (Figure 2). A thiol−thiolate hydrogen bond between Cys284 residues was observed in both AeKAT−cysteine and AeKAT−glutamine complexes as described in the previously reported unliganded structures (PLP form, 3.6 Å; PMP form, 3.5 Å) (*20*), but the thiol−thiolate hydrogen bond (3.7 Å) in the AeKAT−cysteine complex is slightly longer than that in the unliganded structures. However, the structure of the AeKAT−cysteine complex did not provide any clues regarding the potential interaction of free cysteine with the thiol−thiolate hydrogen bond. A mutation study seems necessary to determine if the thiol−thiolate hydorogen bond between Cys284 residues is the cysteine regulation target.

On superposition of chain A onto chain B of the AeKAT−cysteine complex (rmsd = 0.7666 Å) (Figure 3A), we identified the residues within 5 Å of cysteine and found that chain A and chain B differ in the side chain conformations of Trp27, Gln44, Tyr111, Phe391, and Arg405 that tilt or move closer to the substrate cysteine. In particular, the NE2 atom of Gln44 in chain B moved as much as 7.9 Å to form hydrogen bonds with the substrate (Figure 3B). By binding the substrate cysteine, the small domain of chain B rotates toward the cofactor (Figure 3A), which makes most of the residues around the active center closer to the cofactor and encapsulates the substrate within the center. Therefore, chain B has a closed conformation. The built-in cavity at the protein surface is clearly seen as the open form in chain A (Figure 4A), in which a tunnel-like unoccupied space in the cavity appears to serve as the entry path for the substrate. The PLP cofactor can be clearly seen through the tunnel-like structure. In contrast, the tunnel is closed in chain B that contains a cysteine (Figure 4B). The built-in cavity is constructed by the residues at the domain interface and the subunit interface

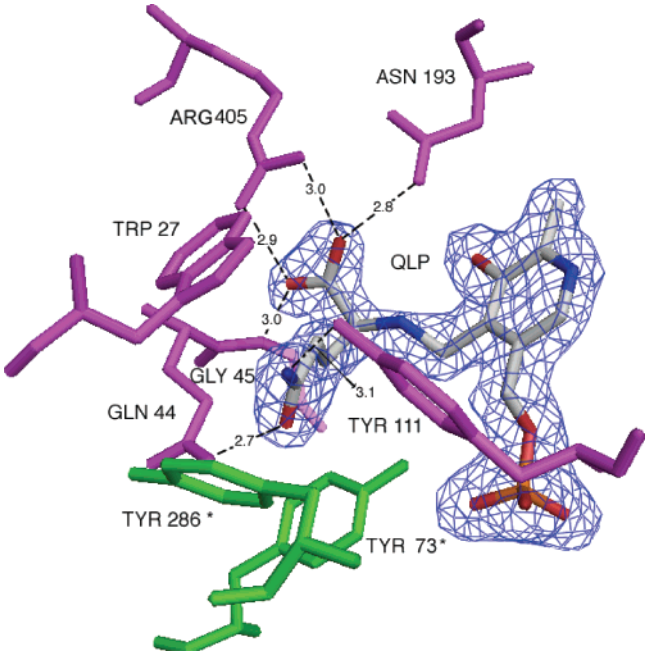

FIGURE 5: Glutamine binding site. The glutaminyl aldimine (QLP) and the protein residues within 4 Å of the glutamine substrate are shown. The residues colored pink are from chain A and residues colored green from chain B. The $2F_o - F_c$ electron density map covering the QLP is shown contoured at the 1.2σ level. This figure was generated with PyMol.

of the enzyme. The main residues building the cavity wall are Leu69, Phe135, Asn193, and Tyr224 from the large domain at chain B, Trp27, Ile31, Ala35, Lys38, Asn41, Gln44, Gly45, Phe46, Phe347, and Arg405 from the small domain at chain B, and Tyr73 and Tyr286 from chain A.

Substrate Recognition and Catalysis in the AeKAT−Glutamine Complex. Similar to the crystal structure of AeKAT−cysteine complex, the substrate lies near the PLP cofactor and forms an external aldimine with PLP in each subunit of the AeKAT−glutamine complex (Figure 5). Several residues, including Arg405, Tyr224, Asn193, Gly45, Trp27, Gln44, Tyr111, and Phe135, define the substrate-binding site and contact the glutamine molecule in both subunits of the biological dimer (Figure 5). Upon superposition of chain A onto chain B of the AeKAT−glutamine complex (rmsd = 0.3263 Å), we determined that both chains have a closed conformation. The interactions between glutamine and protein are basically the same as the interactions between cysteine and protein, with the exception that glutamine has an increased number of interactions. For example, the glutamine R group of QLP is stabilized by hydrogen bonds with the OH atom of Tyr73 (A chain) (3.9 Å), the OH atom of Tyr111 (3.1 Å), and the NE2 atom of Gln44 (2.7 Å), and also through hydrophobic interactions with the ring of Tyr286 (A chain) (3.8 Å). In contrast, the cysteine R group of C6P interacts with only the NE2 atom of Gln44 (3.4 Å).

DISCUSSION

By cocrystallizing with the substrates cysteine, glutamine, kynurenine, and tyrosine, AeKAT was cocrystallized with only an excess of the substrate cysteine, yielding crystals of a true intermediate complex, cysteinyl aldimine. The AeKAT−cysteine complex represents an excellent model of the

Scheme 1: AeKAT-Catalyzed Transamination Reaction

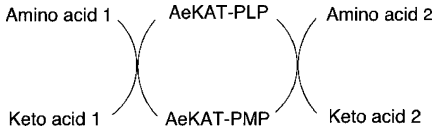

complex structure free from the bias caused by structural differences between substrate analogues (or inhibitors). Cysteine not only is one of the best substrates for AeKAT but also affects enzyme activity toward kynurenine, enhancing kynurenic acid production between 0.6 and 2.5 mM and inhibiting kynurenic acid formation at >5 mM (*5*). The inhibition can be explained by the mechanism of substrate competition, but it is unclear how cysteine increases enzyme activity toward kynurenine. The enzyme is crystallized at 2.5 mM cysteine in the crystallization buffer but is not crystallized at the same concentration of other substrates, which suggests that cysteine may help stabilize the enzyme. Cysteine is found in only one subunit of the biological dimer. In contrast, crystals of the AeKAT−glutamine complex are obtained by soaking the native crystals with glutamine, and glutamine is found in both subunits of the AeKAT−glutamine complex structure. Both cysteine and glutamine are good amino group donors for AeKAT with K_m values of 1.3 mM with cysteine and 3.8 mM with glutamine (*5*). The concentrations of cysteine and glutamine are the same in the cocrystallization buffer and the soaking buffer. Theoretically, cysteine should be somewhat easier than glutamine to bind to the active site of AeKAT based on their affinity for the enzyme. The presence of cysteine in just one of the two subunits as determined by cocrystallization and the presence of glutamine in both subunits as determined by soaking suggest that the kinetic constants of the enzyme are different between crystal and solution forms. This should serve as an example illustrating the different behaviors between crystal and solution forms of an enzyme.

AeKAT conducts ping-pong bi-bi reactions to catalyze keto acid 1 and amino acid 2 to amino acid 1 and keto acid 2, respectively. As shown in Scheme 1, amino acid 1 adds to the AeKAT-PLP form of the enzyme, producing the AeKAT−amino acid 1 complex, but then the enzyme is covalently altered to form a complex between a stable enzyme form, AeKAT-PMP, and the first product of keto acid 1. Keto acid 1 is then ejected, and a second substrate, keto acid 2, adds to the enzyme. The amino group originally transferred to AeKAT-PLP to form AeKAT-PMP is then transferred to keto acid 2, forming amino acid 2 and regenerating the AeKAT-PLP form. Finally, amino acid 2 is ejected, and the cycle is complete (*23*). The fact that cysteine is found in only one subunit of the biological dimer in the cocrystallized crystal structure is interesting. In the complex of *Paracoccus denitrificans* aromatic amino acid aminotransferase with 3-phenylpropionate (*33*) and the complex of *A. aegypti* alanine glyoxylate aminotransferase with alanine (*34*), the substrate also was observed in only one subunit of their homodimers. On the basis of these results, it seems reasonable to suggest that the two subunits of AeKAT are not synchronized during the enzyme-catalyzed reaction through a ping-pong bi-bi mechanism and that the catalyzing mechanism of the aminotransferases might be more complicated than we thought.

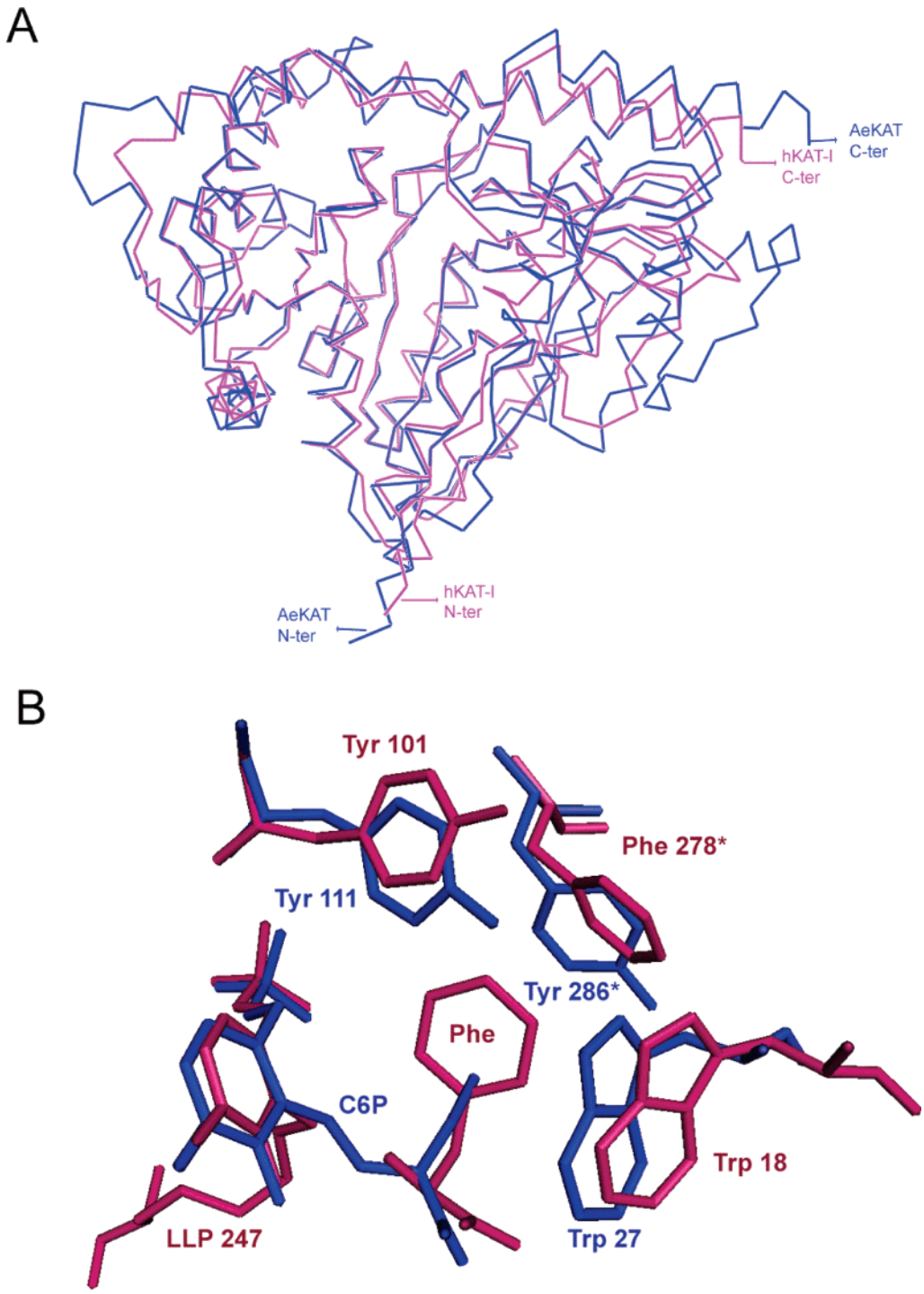

FIGURE 6: (A) α-Carbon representation of the AeKAT−cysteine structure (blue) superimposed onto the hKAT I−phenylalanine structure (pink). (B) Superposition of the AeKAT−cysteine structure onto the hKAT I−phenylalanine structure. Only different protein residues within 5 Å of the cysteine substrate or phenylalanine substrate are depicted as sticks. The residues and ligand form of AeKAT are colored blue and those from hKAT I colored red.

The substrate profiles of AeKAT and hKAT I are essentially the same, including aromatic amino acids (kynurenine, phenylalanine, tryptophan, and tyrosine), sulfur-containing amino acids (methionine and cysteine), and other amino acids (glutamine, leucine, histidine, asparagine, and aminobutyrate). However, they exhibit catalytic efficiencies quite different from those of the amino acids mentioned above. hKAT I is more efficient in transaminating hydrophobic amino acids (such as phenylalanine, leucine, and tryptophan), while AeKAT is more efficient in transaminating relatively hydrophilic amino acids (such as cysteine, histidine, tyrosine, and methionine) (*4*, *5*). Upon superposition of a dimer of the AeKAT−cysteine complex onto the hKAT I−phenylalanine structure (Figure 6A), we identified the residues within 5 Å of both ligands and found that most residues were the same. An exception was that Tyr286 of AeKAT was replaced with Phe278 in hKAT I (Figure 6B). This difference between the two enzymes might explain their difference in terms of catalytic efficiency with hydrophobic and hydrophilic substrates. A sequence alignment shows that

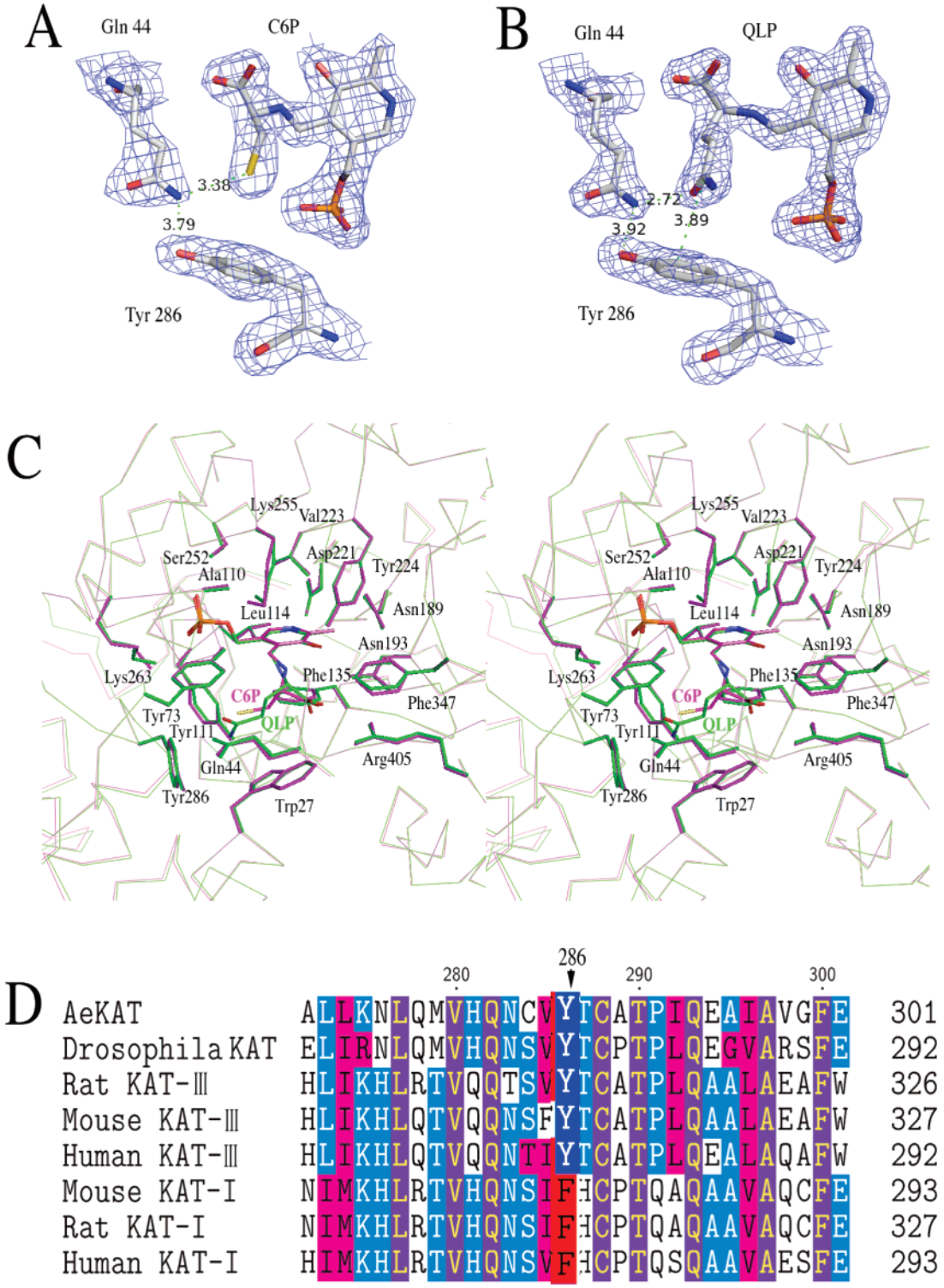

FIGURE 7: (A) Tyr286 in the AeKAT−cysteine structure. The $2F_o - F_c$ electron density map covering C6P, Gln44, and Tyr286 is shown contoured at the 1.2σ level. (B) Tyr286 in the AeKAT−glutamine structure. The $2F_o - F_c$ electron density map covering QLP, Gln44, and Tyr286 is shown contoured at the 1.2σ level. (C) Stereo α-carbon representation of the AeKAT−cysteine complex (pink) superimposed onto the AeKAT−glutamine complex (green). The active site residues within 4 Å of the substrate are shown as sticks. (D) Sequence alignment of *Drosophila* KAT and AeKAT with KAT I and KAT III sequences from mouse, rat, and human. Tyr286 in AeKAT and the aligned residues in other KATs are highlighted.

KAT I sequences from different mammalian species have a Phe residue in this position, but insect KAT and mammalian KAT III sequences have Tyr residue at the same site (Figure 7D). Upon superposition of an AeKAT−cysteine complex ligand binding chain onto a chain of the AeKAT−glutamine complex (Figure 7C), we did not observe any significant conformational changes in the two structures. Inspection of the electron density map indicates that the OH atom of Tyr286 can interact with the NE2 atom of Gln44, which in turn may impact substrate binding (Figure 7A,B). Therefore, the Tyr286 at the active site of AeKAT might enhance the binding of relatively hydrophilic substrates, while the cor-

responding Phe residue at the same position might better interact with relatively hydrophobic substrates. However, the difference (tyrosine vs phenylalanine) does not seem to change the substrates of the KAT enzymes, because AeKAT and human KAT I possess the same substrate profiles.

It is well-known that by binding its substrates, aspartate aminotransferase changes its conformation from the open form to the closed form (*35*−*40*). This substrate-mediated conformation change is also observed in other aminotransferases (*21*, *33*, *41*). The AeKAT−cysteine and AeKAT−glutamine structures show that the protein subunits are crystallized as closed forms when they bind substrates. It is possible that the approach of cysteine or glutamine to the built-in cavity, which is exposed to the solvent region, induces movement of a subdomain (small domain here) toward the large domain. By doing so, the enzyme encapsulates the substrate within the cavity to produce a Michaelis complex. Therefore, all the residues on the cavity wall, instead of only the binding residues, might be collectively involved in the substrate-mediated conformation change and substrate binding.

ACKNOWLEDGMENT

This work was carried out in part at the National Synchrotron Light Source, Brookhaven National Laboratory.

REFERENCES

1. Yu, P., Li, Z., Zhang, L., Tagle, D. A., and Cai, T. (2006) Characterization of kynurenine aminotransferase III, a novel member of a phylogenetically conserved KAT family, *Gene 365*, 111−118.
2. Schwarcz, R. (2004) The kynurenine pathway of tryptophan degradation as a drug target, *Curr. Opin. Pharmacol. 4*, 12−17.
3. Cooper, A. J. (2004) The role of glutamine transaminase K (GTK) in sulfur and α-keto acid metabolism in the brain, and in the possible bioactivation of neurotoxicants, *Neurochem. Int. 44*, 557−577.
4. Han, Q., Li, J., and Li, J. (2004) pH dependence, substrate specificity and inhibition of human kynurenine aminotransferase I, *Eur. J. Biochem. 271*, 4804−4814.
5. Han, Q., and Li, J. (2004) Cysteine and keto acids modulate mosquito kynurenine aminotransferase catalyzed kynurenic acid production, *FEBS Lett. 577*, 381−385.
6. Hosono, A., Mizuguchi, H., Hayashi, H., Goto, M., Miyahara, I., Hirotsu, K., and Kagamiyama, H. (2003) Glutamine:phenylpyruvate Aminotransferase from an Extremely Thermophilic Bacterium, *Thermus thermophilus* HB8, *J. Biochem. (Tokyo) 134*, 843−851.
7. Leeson, P. D., and Iversen, L. L. (1994) The glycine site on the NMDA receptor: structure-activity relationships and therapeutic potential, *J. Med. Chem. 37*, 4053−4067.
8. Perkins, M. N., and Stone, T. W. (1982) An iontophoretic investigation of the actions of convulsant kynurenines and their interaction with the endogenous excitant quinolinic acid, *Brain Res. 247*, 184−187.
9. Birch, P. J., Grossman, C. J., and Hayes, A. G. (1988) Kynurenic acid antagonises responses to NMDA via an action at the strychnine-insensitive glycine receptor, *Eur. J. Pharmacol. 154*, 85−87.
10. Pereira, E. F., Hilmas, C., Santos, M. D., Alkondon, M., Maelicke, A., and Albuquerque, E. X. (2002) Unconventional ligands and modulators of nicotinic receptors, *J. Neurobiol. 53*, 479−500.
11. Hilmas, C., Pereira, E. F., Alkondon, M., Rassoulpour, A., Schwarcz, R., and Albuquerque, E. X. (2001) The brain metabolite kynurenic acid inhibits α7 nicotinic receptor activity and increases non-α7 nicotinic receptor expression: Physiopathological implications, *J. Neurosci. 21*, 7463−7473.
12. Alkondon, M., Pereira, E. F., Yu, P., Arruda, E. Z., Almeida, L. E., Guidetti, P., Fawcett, W. P., Sapko, M. T., Randall, W. R., Schwarcz, R., Tagle, D. A., and Albuquerque, E. X. (2004) Targeted deletion of the kynurenine aminotransferase ii gene reveals a critical role of endogenous kynurenic acid in the regulation of synaptic transmission via α7 nicotinic receptors in the hippocampus, *J. Neurosci. 24*, 4635−4648.
13. Wang, J., Simonavicius, N., Wu, X., Swaminath, G., Reagan, J., Tian, H., and Ling, L. (2006) Kynurenic acid as a ligand for orphan G protein-coupled receptor GPR35, *J. Biol. Chem. 281*, 22021−22028.
14. Mellor, A. L., and Munn, D. H. (2004) IDO expression by dendritic cells: Tolerance and tryptophan catabolism, *Nat. Rev. Immunol. 4*, 762−774.
15. Taylor, M. W., and Feng, G. S. (1991) Relationship between interferon-γ, indoleamine 2,3-dioxygenase, and tryptophan catabolism, *FASEB J. 5*, 2516−2522.
16. Stone, T. W., and Darlington, L. G. (2002) Endogenous kynurenines as targets for drug discovery and development, *Nat. Rev. Drug Discovery 1*, 609−620.
17. Han, Q., Fang, J., and Li, J. (2001) Kynurenine aminotransferase and glutamine transaminase K of *Escherichia coli*: Identity with aspartate aminotransferase, *Biochem. J. 360*, 617−623.
18. Fang, J., Han, Q., and Li, J. (2002) Isolation, characterization, and functional expression of kynurenine aminotransferase cDNA from the yellow fever mosquito, *Aedes aegypti*(1), *Insect Biochem. Mol. Biol. 32*, 943−950.
19. Rossi, F., Han, Q., Li, J., Li, J., and Rizzi, M. (2004) Crystal structure of human kynurenine aminotransferase I, *J. Biol. Chem. 279*, 50214−50220.
20. Han, Q., Gao, Y. G., Robinson, H., Ding, H., Wilson, S., and Li, J. (2005) Crystal structures of *Aedes aegypti* kynurenine aminotransferase, *FEBS J. 272*, 2198−2206.
21. Goto, M., Omi, R., Miyahara, I., Hosono, A., Mizuguchi, H., Hayashi, H., Kagamiyama, H., and Hirotsu, K. (2004) Crystal Structures of Glutamine:Phenylpyruvate Aminotransferase from *Thermus thermophilus* HB8: Induced Fit and Substrate Recognition, *J. Biol. Chem. 279*, 16518−16525.
22. Jansonius, J. N. (1998) Structure, evolution and action of vitamin B6-dependent enzymes, *Curr. Opin. Struct. Biol. 8*, 759−769.
23. Eliot, A. C., and Kirsch, J. F. (2004) Pyridoxal phosphate enzymes: Mechanistic, structural, and evolutionary considerations, *Annu. Rev. Biochem. 73*, 383−415.
24. Otwinowski, Z. (1993) in *HKL User's Manual* (Sawyer, L., Isaacs, N., and Bailey, S., Eds.) pp 56−62, Daresbury Laboratory, Warrington, U.K.
25. Minor, W. (1993) Ph.D. Dissertation, Purdue University, West Lafayette, IN.
26. Vagin, A., and Teplyakov, A. (1997) MOLREP: An automated program for molecular replacement, *J. Appl. Crystallogr. 30*, 1022−1025.
27. Murshudov, G. N., Vagin, A. A., and Dodson, E. J. (1997) Refinement of macromolecular structures by the maximum-likelihood method, *Acta Crystallogr. D53*, 240−255.
28. Jones, T. A., Zou, J. Y., Cowan, S. W., and Kjeldgaard, M. (1991) Improved methods for building protein models in electron density maps and the location of errors in these models, *Acta Crystallogr. A47* (Part 2), 110−119.
29. Perrakis, A., Sixma, T. K., Wilson, K. S., and Lamzin, V. S. (1997) wARP: Improvement and extension of crystallographic phases by weighted averaging of multiple refined dummy atomic models, *Acta Crystallogr. D53*, 448−455.
30. Kabsch, W. (1976) Crystal Physics, Diffraction, Theoretical and General Crystallography, *Acta Crystallogr. A32*, 922−923.
31. DeLano, W. L. (2002) *PyMol*, DeLano Scientific, San Carlos, CA.
32. Laskowski, R. A., Macarthur, M. W., Moss, D. S., and Thornton, J. M. (1993) Procheck: A Program to Check the Stereochemical Quality of Protein Structures, *J. Appl. Crystallogr. 26*, 283−291.
33. Okamoto, A., Nakai, Y., Hayashi, H., Hirotsu, K., and Kagamiyama, H. (1998) Crystal structures of *Paracoccus denitrificans* aromatic amino acid aminotransferase: A substrate recognition site constructed by rearrangement of hydrogen bond network, *J. Mol. Biol. 280*, 443−461.
34. Han, Q., Robinson, H., Gao, Y. G., Vogelaar, N., Wilson, S. R., Rizzi, M., and Li, J. (2006) Crystal Structures of *Aedes aegypti* Alanine Glyoxylate Aminotransferase, *J. Biol. Chem. 281*, 37175−37182.
35. Rhee, S., Silva, M. M., Hyde, C. C., Rogers, P. H., Metzler, C. M., Metzler, D. E., and Arnone, A. (1997) Refinement and comparisons of the crystal structures of pig cytosolic aspartate aminotransferase and its complex with 2-methylaspartate, *J. Biol. Chem. 272*, 17293−17302.

36. Miyahara, I., Hirotsu, K., Hayashi, H., and Kagamiyama, H. (1994) X-ray crystallographic study of pyridoxamine 5′-phosphate-type aspartate aminotransferases from *Escherichia coli* in three forms, *J. Biochem. (Tokyo) 116*, 1001−1012.
37. Malashkevich, V. N., Strokopytov, B. V., Borisov, V. V., Dauter, Z., Wilson, K. S., and Torchinsky, Y. M. (1995) Crystal structure of the closed form of chicken cytosolic aspartate aminotransferase at 1.9 Å resolution, *J. Mol. Biol. 247*, 111−124.
38. McPhalen, C. A., Vincent, M. G., and Jansonius, J. N. (1992) X-ray structure refinement and comparison of three forms of mitochondrial aspartate aminotransferase, *J. Mol. Biol. 225*, 495−517.
39. Okamoto, A., Higuchi, T., Hirotsu, K., Kuramitsu, S., and Kagamiyama, H. (1994) X-ray crystallographic study of pyridoxal 5′-phosphate-type aspartate aminotransferases from *Escherichia coli* in open and closed form, *J. Biochem. (Tokyo) 116*, 95−107.
40. Jager, J., Moser, M., Sauder, U., and Jansonius, J. N. (1994) Crystal structures of *Escherichia coli* aspartate aminotransferase in two conformations. Comparison of an unliganded open and two liganded closed forms, *J. Mol. Biol. 239*, 285−305.
41. Hirotsu, K., Goto, M., Okamoto, A., and Miyahara, I. (2005) Dual substrate recognition of aminotransferases, *Chem. Rec. 5*, 160−172.

BI701800J